1st National Applied Mechanisms & Robotics Conference,
Cincinnati, Ohio, Nov. 5-8, 1989, 89AMR-3A-3, Volume I.

# AUTONOMOUS RECTILINEAR MOTION PLANNING
## Part II: The Geometry of the End-Effector Workspace and Determination of a Free Path

Menq-Dar Shieh
Research Assistant

Joseph Duffy
Graduate Research Professor
Department of Mechanical Engineering
Director
Center for Intelligent Machines and Robotics
University of Florida
Gainesville, Florida 32611

**ABSTRACT**

In this second paper the analysis of the Reachable Area (**RA**) of the wrist point in the previous paper is extended to determine the **RA** of a point in the end effector for a single circular obstacle.

A time-efficient algorithm was subsequently developed using the geometry of the manipulator workspace for determining a collision free rectilinear motion of the end effector of a planar 3R manipulator with a single circular obstacle inside the workspace.

The algorithms developed for this work were successfully implemented using the Silicon Graphics 4D system.

The execution time for determining the possibility of a rectilinear motion from an initial to a final position was within 1 second. If such rectilinear motion was not possible, the algorithm generated a path autonomously consisting of a sequence of line segments. The computer time of this was about 1 second.

**INTRODUCTION**

The Reachable Area (**RA**) of the end-effector facilitates the determination of motion capability simply because it enables one to check whether the target position lies within the **RA** or not. Obviously, if the target point lies within the **RA** of the manipulator, a rectilinear motion from the initial position to the final position is possible.

However, if the target point lies outside the **RA**, the tip of the end effector of the manipulator cannot follow a rectilinear motion to the target point. In this case, the **RA** for the final configuration is determined, and an intermediate point will be suggested within the area created by the intersection of the initial and final **RAs**. However, it can occur that these two **RAs** do not intersect, in which case a free-path is determined using several intermediate points.

The development presented here can be readily extended to determine paths with multiple circular obstacles present in the workspace.

**REACHABLE AREA OF END-EFFECTOR**

It is assumed that the manipulator executes a rectilinear motion with a constant orientation of the end-effector. The **RA** of the end-effector (point 4) (see Fig.1) is identical to that of the wrist (point 3) but is translated a distance $a_{34}\underline{a}_{34}$ (see Lipkin, Torfason, and Duffy [1]). The shaded area, which is inaccessible to the end-effector because of the obstacle, must be subtracted from the translated **RA**.

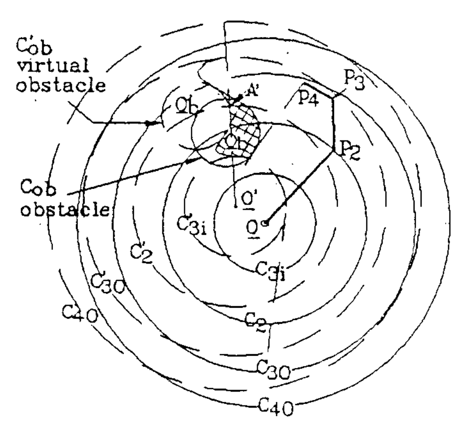


**Figure 1** RA of the End-Effector.

This shaded area is covered by the union of three shaded areas (m), (n), and (s) (see Fig.2).

<u>Shaded Area (m)</u>

The shaded area (m) is bounded by four lines $L_5$, $L_6$, $L_7$, and $L_8$ (Fig.2(a)). Lines $L_5$

and $L_6$, passing through the centers of the obstacle $C_{ob}$ and the virtual obstacle $C_{ob}'$ respectively, are selected to be perpendicular to line $\underline{O}_b\underline{O}_b'$ (or $a_{34}$). Lines $L_7$ and $L_8$ are two common tangent lines to the obstacles. If the origin is moved from $\underline{O}$ to $\underline{O}_m = 0.5 \times (\underline{O}_b + \underline{O}_b')$ (the midpoint of line $\underline{O}_b\underline{O}_b'$), the line equations $L_5$, $L_6$, $L_7$, and $L_8$ become $L_5'$, $L_6'$, $L_7'$, and $L_8'$. The shaded area (m) can be expressed by

$$\overline{M}=(L_5'(\underline{X})<0)\wedge(L_6'(\underline{X})<0)\wedge(L_7'(\underline{X})<0)\wedge(L_8'(\underline{X})<0)=1 \quad (1)$$

<u>Shaded Area (n)</u>

The shaded area (n) is the umbra of the real obstacle with respect to point 4 (Fig.2(b)). $C_{ob}$ is the boundary of the obstacle. $L_9$ is the polar of point $P_4$ with respect to the obstacle. $K_9$ is a degenerate conic, which represents a pair of tangent lines with respect to the obstacle. When the origin is moved from $\underline{O}$ to $\underline{O}_b$, the parameters $C_{ob}$, $L_9$ and $K_9$ are changed into $C_{ob}*$, $L_9'$, and $K_9'$. The shaded area (n) is determined by

$$\overline{M}=(C_{ob}*(\underline{X})<0)\vee[(L_9'(\underline{X})<0)\wedge(K_9'(\underline{X})<0)]=1. \quad (2)$$

<u>Shaded Area (s)</u>

The shaded area (s) is bounded by three lines $N_2$ ($\underline{p}_4\underline{O}_b'$), $N_3$ ($\underline{p}_4\underline{O}_b$), $N_4$ ($\underline{O}_b\underline{O}_b'$) and $C_{30}'$ (Fig.2(c)). The line equations are transformed into $N_2'$, $N_3'$, and $N_4'$ after the origin is shifted from $\underline{O}$ to $\underline{O}_s = 0.5 \times (0.5 \times (\underline{O}_b + \underline{O}_b') + \underline{p}_4)$ (the midpoint of the ray through point 4 which bisects $\underline{O}_b\underline{O}_b'$). The shaded area (s) is defined by

$$\overline{M}=(N_2'(\underline{X})<0)\wedge(N_3'(\underline{X})<0)\wedge(N_4'(\underline{X})>0) = 1. \quad (3)$$

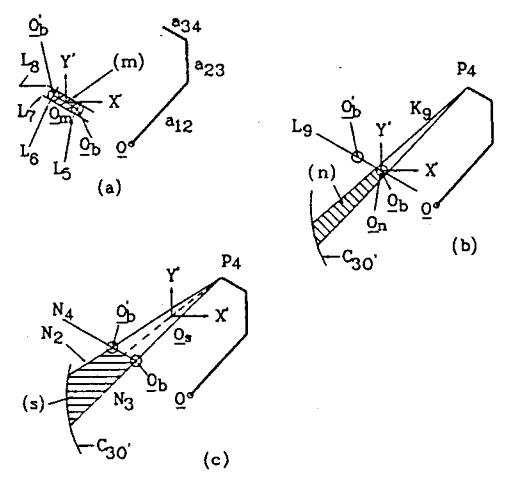


**Figure 2** Determination of **NAs** (m), (n), and (s).

Subtracting these three areas from the translated **RA** in (Fig.1) yields the **RA** of the end-effector (point 4). The calculations for these three shaded areas are thus completely analogous to those for the **RA** of the wrist (point 3) (see part I) and hence no further equations are required for this computation. Also, the translation of the whole **RA** of the wrist is determined by replacing $\underline{X}$ with $\underline{X}-a_{34}\underline{a}_{34}$. The fast determination of the **RA** of the end-effector simplifies the motion planning problem among obstacles.

## INTERSECTION OF TWO REACHABLE WORKSPACES WITH RESPECT TO THE INITIAL AND THE FINAL CONFIGURATIONS

When a starting point and a target point are specified together with the orientation of the end-effector, two configurations (the initial and the final) can be determined as shown in (Fig.3). An **RA** of the end-effector with respect to the initial configuration is constructed (see Fig.4) by using the algorithm given in the previous section. It is apparent that in this example the target point lies outside the **RA** of the initial configuration so that a single rectilinear motion of the end-effector is not possible and one or several intermediate points are needed to construct a path to the target position.

In order to solve the problem, an **RA** of the final configuration is determined (see Fig.5). The intersection of these two **RAs** (Fig.6) is the region where intermediate points can be selected. When there is no intersection of these two **RAs**, it is necessary to move the robot to an intermediate position in the initial **RA** and to determine a corresponding intermediate **RA** which intersects the final **RA**.

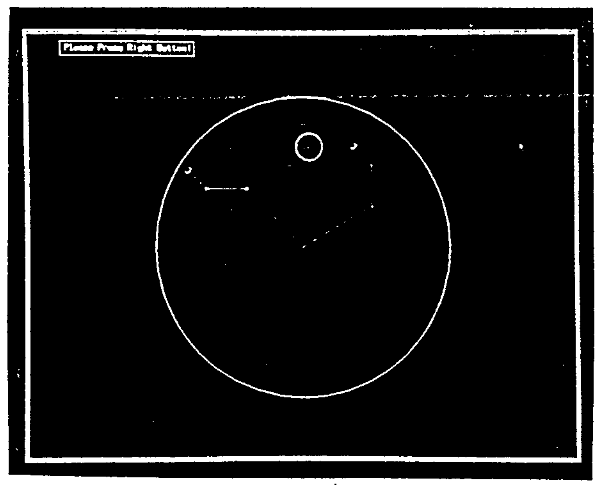

**Figure 3** Initial and Final Configurations of a Planar 3R Manipulator.

## GENERATION OF A FREE PATH BETWEEN TWO POINTS

An automatic search method to determine the intermediate positions is presented in this section. There are three distinct cases which are similar to the Cases (1), (2), and (3) discussed in Part I.

<u>Computation of a free path for case (1)</u>

In this case the second link cannot be a tangent to the obstacle (see Case (1), Part I). There are three subcases which must be considered.

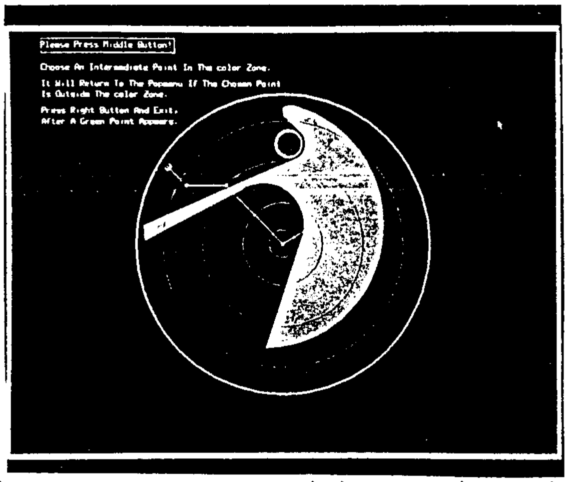

**Figure 4** RA of the Initial Configuration.

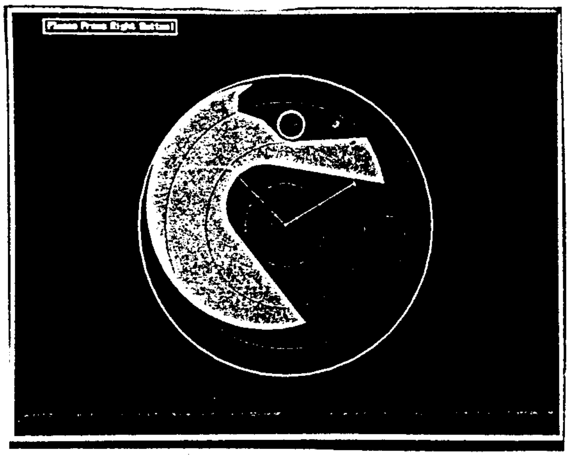

**Figure 5** RA of the Final Configuration.

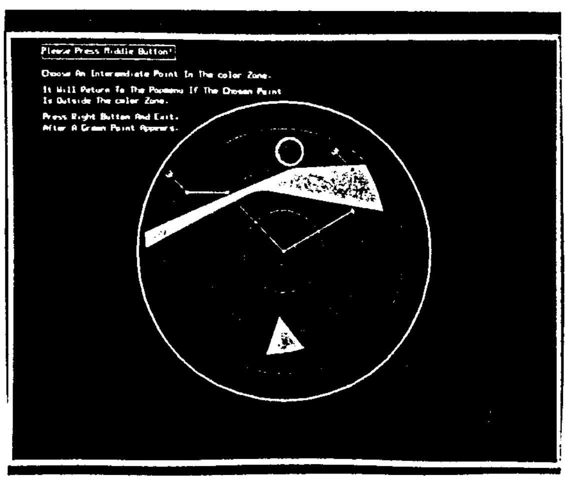

**Figure 6** Intersection of the Initial and Final RAs.

<u>Case (1.1): The target position $q_4$ is in the umbra of the circle $C_{3i}'$.</u> Two branch paths $p_4g_1q_4$ and $p_4g_2q_4$ (see Fig.7) can, however, be chosen as free paths. Two lines tangent to the circle $C_{3i}'$ and passing through points $p_4$ and $q_4$ respectively are drawn (lines $L_4'$ and $L_5'$) which intersect at point $g_1$. A two sided path $p_4g_1q_4$ thus satisfies the required motion. The two other tangents from $p_4$ and $q_4$ intersecting at $g_2$ also satisfy the required motion. The choice of the path may be determined by, for example, selecting the shorter of the lengths $p_4g_1q_4$ and $p_4g_2q_4$.

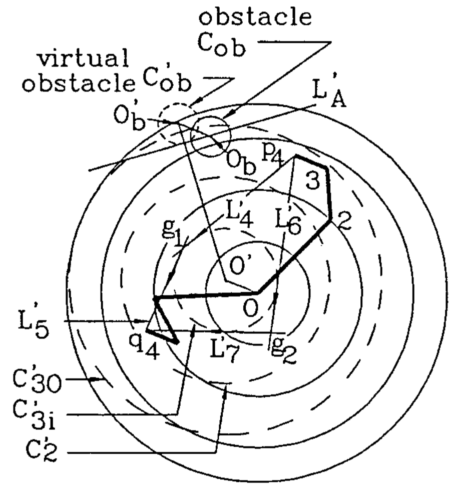


**Figure 7** Determination of the Collision Free Paths of Case (1.1).

<u>Case (1.2): The target position $q_4$ lies inside the shadow of the obstacle $C_{ob}$.</u> In this case an intermediate point $g_3$ (Fig.8) is chosen so that the robot can move from point $p_4$ to $q_4$ through this point. Point $g_3$ is chosen at the intersection of two tangent lines ($L_8'$ and $L_9'$) to the obstacle $C_{ob}$. These two lines pass through points $p_4$ and $q_4$ respectively.

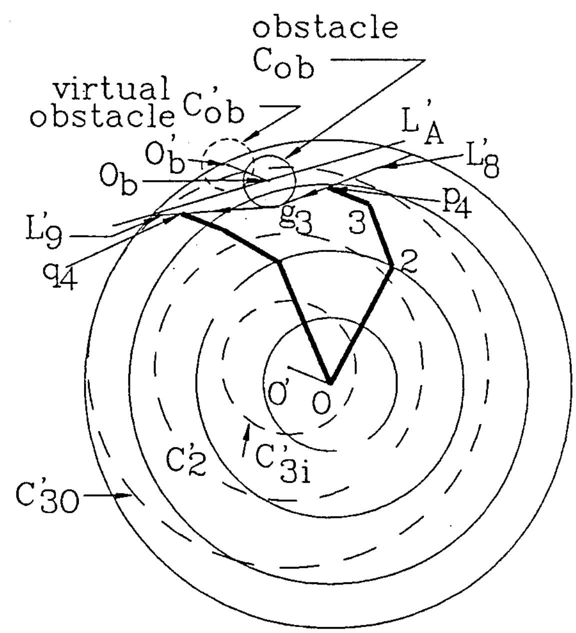


**Figure 8** Determination of the Collision Free Path of Case (1.2).

Case (1.3): Points $p_4$ and $q_4$ and the center of the virtual obstacle ($O_b'$) are on the same side of line $L_A'$[1]. The first step is to move the end-effector away from the obstacle ( from $p_4$ to $p_4'$) (see Fig.9). The next step is to move the end-effector from $p_4'$ to $q_4'$ (see Case (1.1) and (1.2)). The final step is to move the end-effector from $q_4'$ to $q_4$. Points $p_4'$ and $q_4'$ are two intersections of line $L_A'$ and circle $C_{30}'$.

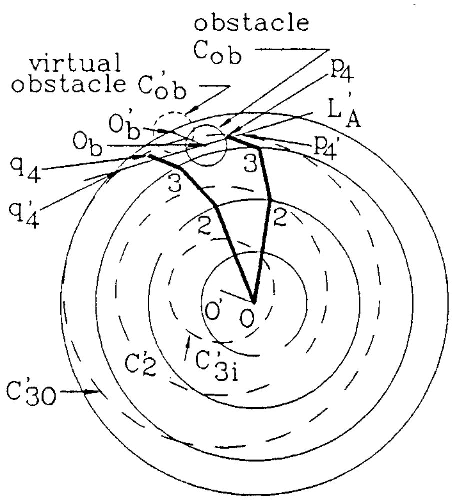


**Figure 9** Determination of the Collision Free Path of Case (1.3).

Computation of a free path for case (2)

In this case the second link can be a tangent to the obstacle and the obstacle lies outside the path of the first link (see Case (2), Part I). There are two subcases which must be considered.

Case(2.1): The target position $q_4$ is in the shadow of the circle $C_{3i}'$ or in the shadow of the obstacle $C_{ob}$. In this case the algorithm is identical to that in Cases (1.1) and (1.2). And points $g_1$, $g_2$, $g_3$ (see Fig 7 and 8) can be chosen as an intermediate point of the free path.

Case (2.2): Point $p_4$ ( or $q_4$ ) and the center of the virtual obstacle ($O_b'$) are on the same side of line $L_2'$[2]. Points $h_1$ and $h_3$ are the intersections of line $L_2'$ and the circle $C_{30}'$ (see Fig.10). Point $h_3$ is chosen to be an intermediate point so that the end-effector of the robot can move from $h_3$ to $q_4$ in the final step.

There are three possible choices for the intermediate point $p_4'$. The first one is point B' (an intersection of line $L_2'$ and circle $C_2'$). The second one is point $h_2$, which is the middle point of line segment $Bh_1$. This can be chosen to be an intermediate point when point B' is not available, viz. when B' lies inside the obstacle $C_{ob}$. The third choice is point $h_1$. This can be chosen as an intermediate point when both points B' and $h_2$ are inside the obstacle.

If point $p_4$ cannot move directly to any of these three points, points $h_4$ and $h_5$ on the circular arc $e_1h_1$ [3] (see Fig.10) can be determined as the intermediate points of the free path $p_4h_4h_5h_1$ to point $h_1$, where $e_1h_4 = h_4h_5 = h_5h_1$.

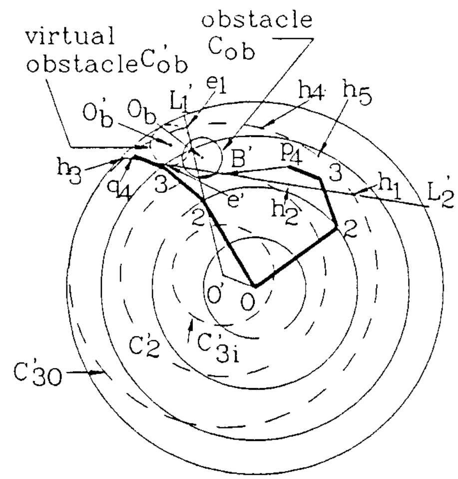


**Figure 10** Determination of the Collision Free Path of Case (2.2).

Computation of a free path for case (3)

In this case link $a_{12}$ can interfere with the obstacle during a specified motion (see Case (3), Part I). There are six subcases which must be considered.

Case (3.1): The initial position $p_4$ and the target position $q_4$ belong to two different zones or point $q_4$ lies in the shadow of circle $C_{3i}'$. Point $g_3$, an intersection of the two tangent lines $L_8'$ and $L_9'$, is chosen to be an intermediate point (see Fig.11(a)). These two lines pass through points $p_4$ and $q_4$ respectively.

Case (3.2): Obstacle $C_{ob}$ lies in the path of the motion. Point $g_4$ (see Fig.11(b)) is selected to be an intermediate point which is the intersection of the two tangent lines $L_4'$ and $L_5'$.

Case (3.3): Point $q_4$ lies in the shadow of the virtual obstacle $C_{obv}'$. Point $g_5$ (see Fig.11(c)) is chosen to be an intermediate point so that the robot can move from $p_4$ to $q_4$ through point $g_5$. Point $g_5$ is the intersection of the two tangent lines $L_6'$ and $L_7'$.

---

[1] Line $L_A'$ (see Fig.9) is a tangent line to the virtual obstacle $C_{ob}'$ with the tangency between points $O_b'$ and O', and is perpendicular to line $O'O_b'$.

[2] $L_2'$ is tangent to the virtual obstacle $C_{ob}'$ at point e' and intersects circle $C_2'$ at B' where $e'B' = a_{23}$ (see Case (2), Part I).

[3] Point $e_1$ is an intersection of line $L_1'$ and the circle $C_{30}'$, which is closest to the virtual obstacle $C_{ob}'$. Line $L_1'$ is drawn from O' and tangent to $C_{ob}'$ on the right side.

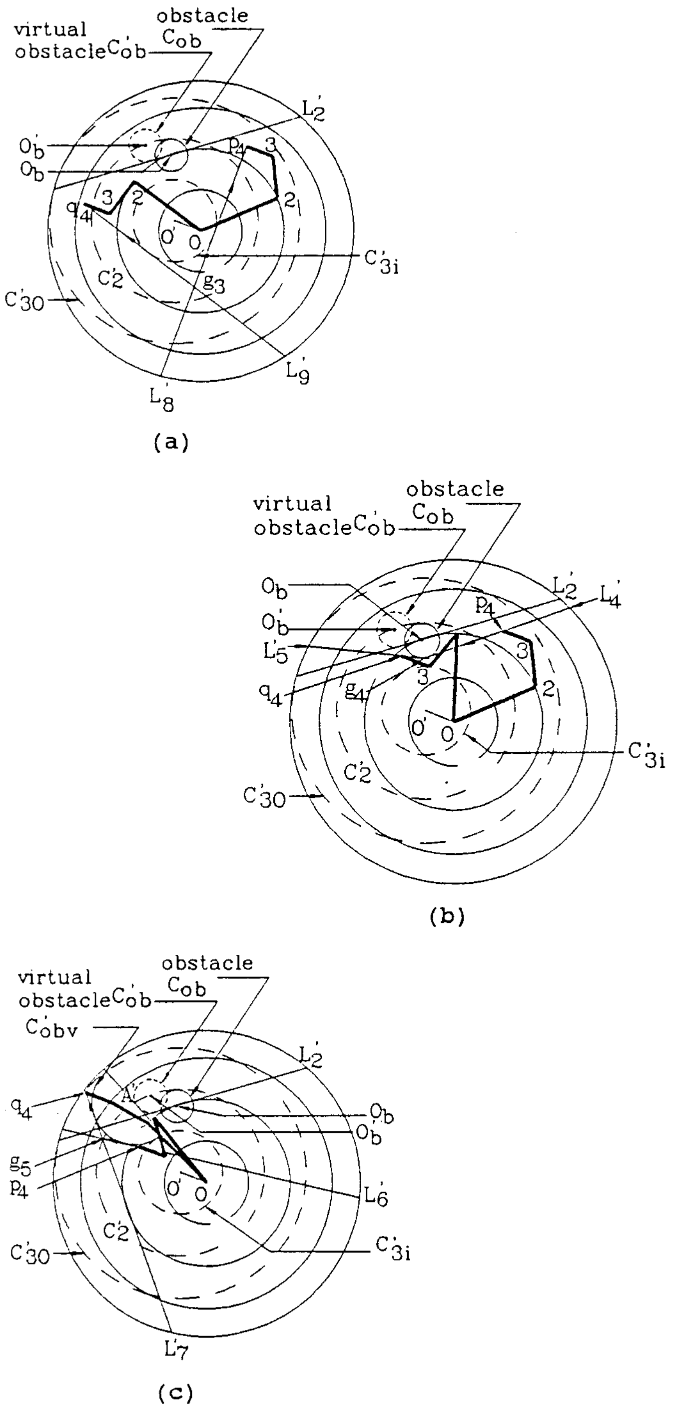


**Figure 11** Determination of the Collision Free Paths of Cases (3.1), (3.2), and (3.3).

<u>Case (3.4): Point $p_4$ and the center of the virtual obstacle ($O_b'$) are on the same side of line $L_2'$.</u> It is necessary to chose an intermediate point on line $L_2'$ so that the algorithms in Cases (3.1), (3.2), and (3.3) can be used. At the outset, there are three choices for the intermediate point $p_4'$ (points B', $h_2$ and $h_1$). These are identical to those discussed in Case (2.2). However, the choice must depend on where the target position $q_4$ is. For example, when the initial and final configurations are in zone(I) (see Fig.12), point B' is the best choice for an intermediate point. Then the determination of the rectilinear motion from B' to $q_4$ is identical to Case (3.1) through Case (3.3). The second choice is point $h_2$, which is the middle point of line segment $Bh_1$. This can be chosen to be an intermediate point when point B' lies inside the obstacle $C_{ob}$.

If the initial and final configurations belong to two different zones, point $h_1$ is the best choice for an intermediate point.

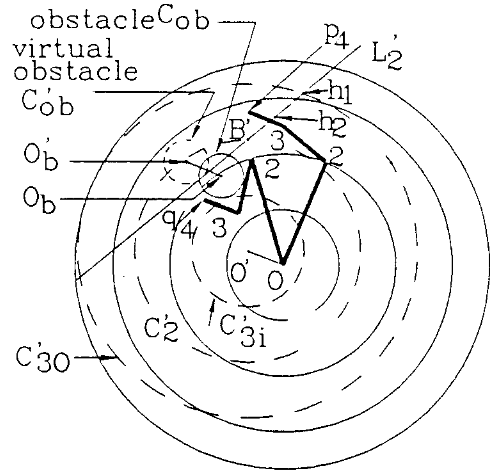


**Figure 12** Determination of the Collision Free Path of Case (3.4).

<u>Case(3.5): Points $q_4$ and $O_b'$ are on the same side of line $L_2'$.</u> Point $q_4'$, an intersection of line $L_2'$ and circle $C_{30}'$, is chosen to be an intermediate point, which is the nearest to the target point $q_4$ (see Fig.13). When the robot cannot move from $q_4'$ directly to point $q_4$, an intermediate point $h_3$ on circle $C_{30}'$ is chosen to generate a free path from $q_4'$ to $q_4$, where $q_4'h_3 = h_3e_1'$ [4].

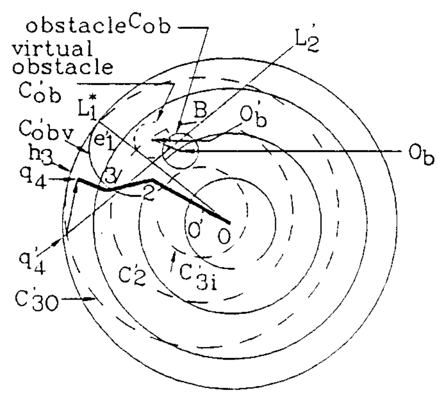


**Figure 13** Determination of the Collision Free Path of Case (3.5).

<u>Case (3.6): Line $L_2'$ does not exist.</u> When $O\,O_b < a_{12} - (a_{23}^2+r^2)^{1/2}$, line $L_2'$ does not exist.

[4] Point $e_1'$ is an intersection of line $L_1^*$ and the circle $C_{30}'$, which is closest to the virtual obstacle $C_{ob}'$. Line $L_1^*$ is drawn from O' and tangent to $C_{ob}'$ on the left side.

Line $L_C'$ is determined (Fig.14), which is tangent to the virtual obstacle $C_{ob}'$ and is perpendicular to line $\underline{O}'\underline{O}_b'$ with the tangency between points $\underline{O}'$ and $\underline{O}_b'$. The determination of the intermediate points is identical to those in Cases (3.1) through (3.5).

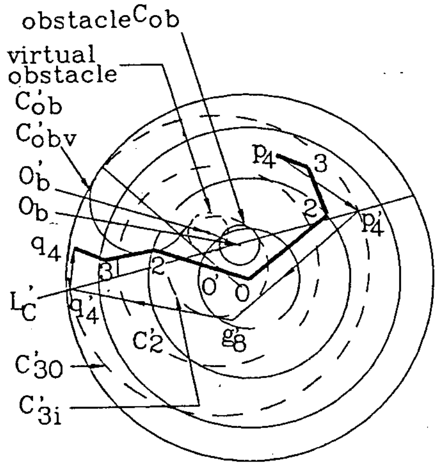


**Figure 14** Determination of the Collision Free Path of Case (3.6).

**SIMULATION OF THE ALGORITHM OF THE OBSTACLE AVOIDANCE OF A PLANAR 3R ROBOT**

The obstacle avoidance algorithms developed in this paper have been successfully implemented using the Silicon Graphics 4D system in CIMAR Laboratory. The link lengths of the planar 3R robot were selected as follows $a_{12} = 30.0$ units, $a_{23} = 15.0$ units and $a_{34} = 10.0$ units.

Figs. 15 and 16 show the results of the rectilinear motion planning for case(2) and case(3) respectively. The algorithm generates a path autonomously and it takes about 1 second of the computer time in the Silicon Graphics 4D system.

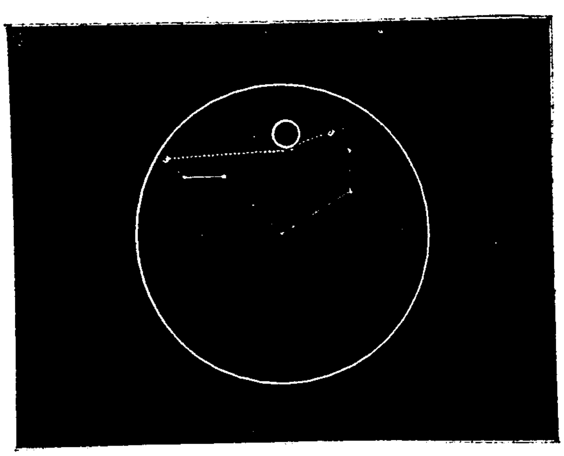

**Figure 15** Collision Free Path of Case (2).

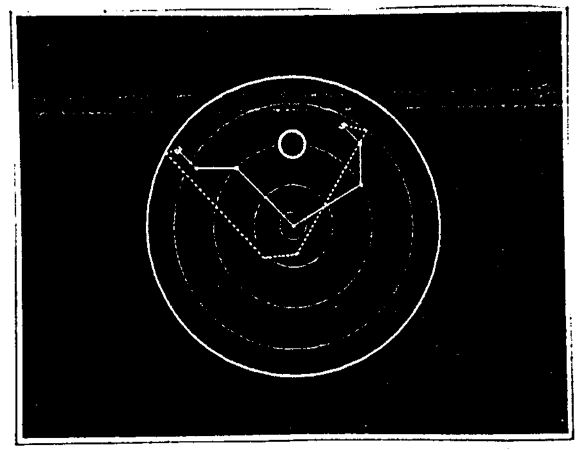

**Figure 16** Collision Free Path of Case (3).

**CONCLUSION AND FUTURE WORK**

A time-efficient algorithm concerning the motion planning of a planar 3R robot with an obstacle inside its workspace has been developed. An effective checking procedure without using the stepped-move approach and the swept-volume calculation is applied to enable a fast determination of a free path around the obstacle. Further studies could elaborate this algorithm; for example, multiple obstacles inside the workspace. In this case the **RA** of a robot configuration can be defined as the common area of the **RAs** of different obstacles.

An important extension of this algorithm is its applications in articulating the links of some spatial robots to guide the end-effector through horizontal tubes or piping.


**ACKNOWLEDGEMENT**

The authors wish to acknowledge the financial support of the Department of Energy (Grant No. DE-FG02-86NE37967).


**REFERENCES**


1. Lipkin H., Torfason L. E., and Duffy J., "Efficient Motion Planning for a Planar Manipulator Based on Dexterity and Workspace Geometry," Conference on Mechanisms and Machinery, Cranfield Institute of Technology, Cranfield, United Kingdom, September 1985.